Graphene on silicon: Effects of the silicon surface orientation on the work function and carrier density of graphene

Y. W. Sun [1,2,*] D. Holec [3,†] D. Gehringer,[3] L. Li,[4] O. Fenwick [1] D. J. Dunstan [5] and C. J. Humphreys[1,‡]

[1]*School of Engineering and Materials Science, Queen Mary University of London, London E1 4NS, United Kingdom*
[2]*School of Chemical Engineering, University of Birmingham, Birmingham B15 2TT, United Kingdom*
[3]*Department of Materials Science, Montanuniversität Leoben, Leoben 8700, Austria*
[4]*College of Information Science and Electronic Engineering, Zhejiang University, Hangzhou 310027, China*
[5]*School of Physics and Astronomy, Queen Mary University of London, London E1 4NS, United Kingdom*

(Received 15 May 2021; revised 26 January 2022; accepted 5 April 2022; published 13 April 2022)

Density functional theory has been employed to study graphene on the (111), (100), and (110) surfaces of bare silicon (Si) substrates, which provide three different densities of surface atoms. There are several interesting findings. First, carbon atoms in graphene can form covalent bonds with Si atoms, when placed close enough on Si (111) and (100) surfaces, but not on the (110) surface. The Si (111) surface shifts the Fermi level of graphene into its conduction band, resulting in an increase of the electron density by three orders of magnitude. The work function of graphene is increased by 0.29 eV on the (111) surface, likely due to the surface dipole from the redistribution of π orbitals. The change in the number of available states below the Fermi level of graphene due to its interaction with the Si surface, is the main cause for the unconventional doping reported in this paper. The electron density can also be increased by eighty times on a Si (100) substrate without the shift of Fermi level, which is another clear example of the proposed doping mechanism. These striking effects that different orientations of a silicon substrate can have on the properties of graphene are related to the surface atom density of the substrate. These results provide valuable guidance to the growth of graphene on Si for various purposes for electronic devices.

DOI: 10.1103/PhysRevB.105.165416

I. INTRODUCTION

The extraordinary properties of graphene reported in the literature are almost always measured for graphene on a substrate [1]. Large-area graphene is usually grown by chemical vapour deposition (CVD) on a copper substrate, the copper acting as a catalyst to decompose the growth gases [2]. However, recently large-area graphene has been grown directly on a sapphire substrate, with no metal catalyst, using high-temperature CVD [3] and metal organic chemical vapour deposition (MOCVD) [4]. This raises the intriguing possibility that catalyst-free and transfer-free large-area graphene could be grown directly on silicon and other substrates using the above techniques. When GaN-on-silicon devices are grown using MOCVD, prior to the growth of the GaN the native silicon oxide layer is removed in the growth chamber by heating the silicon in a hydrogen atmosphere, so that the GaN is grown on a bare silicon surface [5]. This is generally the case for all epitaxial growth on silicon. Similarly, when graphene is grown on silicon using MOCVD, the silicon oxide layer would first be removed. In this paper we theoretically study the interface structure of monolayer graphene on three different bare silicon surfaces: (100), (110), and (111), and hence investigate whether the direct growth of graphene on silicon is possible. In particular, we have studied the spacing between the graphene and the silicon surface, and whether the carbon and silicon atoms form covalent bonds. These three surfaces provide three different densities of surface atoms, a key parameter in this study to which we relate the interfacial states and properties of graphene.

The nature of the interface affects the work function and the carrier density of graphene, which are key properties for electronic and photoelectric devices [6,7]. Calculations reported the work function of freestanding graphene in vacuum to be around 4.5 eV [8]. Experimentally the work function of graphene has been measured on SiO_2 and the values vary from 4.6 to 5.2 eV [9–12]. The higher values were attributed to hydroxyl groups at the SiO_2 surface, presumably from atmospheric water vapour [13,14]. These values further vary with different metal contacts [10]. It is common to dope graphene to tune its work function for specific applications [15,16], such as increasing the power conversion efficiency of a graphene-Si solar cell [17]. In this paper, we quantify the changes of the work function of graphene caused by the mere presence of Si substrates of different surface orientations.

The carrier density of pristine undoped graphene is low as the density of states (DOS) around the Fermi level (at the Dirac point) is low [1]. The theoretical value at 300 K is about 10^{11} cm^{-2} (about 10^{18} cm^{-3} considering graphene to be 3.4 Å thick [18], as expected for a semi-metal) [19], compared to 9.65×10^{9} cm^{-3} for Si [20], 2.33×10^{13} cm^{-3}

*yiwei.sun@qmul.ac.uk
†david.holec@unileoben.ac.at
‡c.humphreys@qmul.ac.uk

for germanium (semiconductors) [21], and 8.49×10^{22} cm^{-3} for copper (metal) from the simple Drude model. These theoretical values are generally consistent with experimental measurements. For example, the experimental value for intrinsic Si is 1.0×10^{10} cm^{-3} [20]. However, the measured value of graphene is usually at least two orders of magnitude higher than the theoretical value, which can be due to substrates, defects, and metal electrode contacts [22].

This paper presents purely theoretical results. It quantifies the effects of different surface orientations of Si substrates on graphene, in the formation of interfacial bonds, work function and carrier density. We relate these effects to the surface atom density and demonstrate the underlying physics. There is a caveat that the modelled systems may deviate from reality due to the limitations and approximations in the DFT calculations, specifically the required large in-plane strain and the bandgap that can result. We discuss the effects (of these necessary in-plane strain and resulting bandgap of graphene) in detail in the following sections. One should therefore be cautious when comparing in detail our theoretical values with the results of future experiments.

II. METHODS

We modelled monolayer graphene on a Si substrate with three different surface orientations, (111), (100), and (110). The simulation box contained 18 C atoms and 36 Si atoms for graphene on Si (111), 20 C atoms and 52 Si atoms for graphene on Si (100), and 30 C atoms and 75 Si atoms for graphene on Si (110). The bottom layers of Si atoms were fixed at the Si lattice constant and the top layers were relaxed. For example, for Si (111), we fixed two and a half double-layers at the bottom, and relaxed the top two double-layers. The in-plane dimensions of the simulation box were kept constant. The surface atom densities are 0.46 (double plane), 0.27 and 0.094 atom/Å^2, for the (111), (100), and (110) surface, respectively. The surface area of the simulation box is not large enough to undergo the usual (7×7) reconstructions, and no other surface reconstruction is seen.

Graphene was strained to the Si lattice on each surface to meet the in-plane periodic boundary condition required for the calculations. Graphene is at 4.6% isotropic tensile strain on Si (111). Anisotropic strain is introduced on other surfaces. For example, some C-C bonds are under 1.2% compressive strain and others under 3.2% tensile strain for graphene on Si (110). These are large strains, which are not a practical representation of the physical system. We will focus on the effects of the substrates by comparing the graphene on the Si surface with graphene similarly strained but free standing. The effects of the in-plane strain are shown in Table I, from which we see a significant increase in work function and a trivial change in carrier density by the imposed strain. And a bandgap opens up with anisotropic strain. These will be discussed in detail in the following sections. In the initial stacking, some C atoms were located directly on top of some Si atoms. The structures were then relaxed while keeping in-plane lattice parameters fixed (thus simulating a thick Si substrate). On the Si (111) surface, where the relaxed structure possesses high symmetry, five more random initial stackings (i.e., random initial in-plane displacement of the graphene sheet) were introduced. The relaxation process includes the in-plane translation of graphene (but no change in strain), and therefore all the structures presented in Fig. 1 are at local energy minima, if not global.

TABLE I. The difference between the calculated Fermi level and electrostatic potential energy at vacuum, which we interpret as the work function are listed for unstrained pristine graphene, graphene strained to Si surfaces but unsupported, and strained graphene with the corresponding Si surface beneath. On each surface, there are two structures relaxed from two different initial separations between graphene and Si. The calculated distance of the Fermi level from the edge of the valence or conduction band, whichever is closer, and the carrier density in the graphene are also listed. The closer band edge is labeled, "C" for the conduction band and "V" for the valence band. Electron density is indicated by n and hole density by p.

	$E_F - E$		
Si surface	Work function (eV)	(edge of band) (eV)	Carrier density (cm^{-2})
Pristine graphene	4.22	0 (V)	$n = 1\times10^{11}$
			$p = 1\times10^{11}$
Strained to Si (111)	4.60	0 (C)	$n = 1\times10^{11}$
			$p = 1\times10^{11}$
On Si (111) 4.0 Å	4.86	0.7 (C)	$n = 2\times10^{13}$
On Si (111) 1.5 Å	4.89	0.6 (C)	$n = 1\times10^{14}$
Strained to Si (100)	4.81	0 (V)	$p = 1\times10^{11}$
On Si (100) 4.0 Å	4.92	0.08 (V)	$n = 2\times10^{10}$
On Si (100) 1.5 Å	5.02	0 (V)	$p = 8\times10^{12}$
Strained to Si (110)	4.62	0 (V)	$p = 2\times10^{11}$
On Si (110) 4.0 Å	4.78	0 (V)	$p = 3\times10^{11}$
On Si (110) 1.5 Å	4.79	0 (V)	$p = 3\times10^{11}$

We wish to know if stable covalent bonds can be formed when the graphene is grown, or deposited, on a Si surface. We note that the separation of van der Waals (vdW) bonded graphene layers in graphite is 3.4 Å and the bond length of SiC in the very stiff 6H-SiC is 1.9 Å [23]. On each surface orientation we therefore relaxed our structure from two different initial graphene-Si separations: 4.0 Å and 1.5 Å. The graphene-Si separation is defined as follows. The position of a graphene plane was defined by the centres of the four C atoms at corners of the plane in a simulation box. The distance from this plane to the centres of the topmost Si atoms is defined as the graphene-Si separation, as shown in Fig. 1. The initial separation of 1.5 Å simulates the close approach of carbon atoms to Si, that could be reached under the high graphene growth temperature [2], while 4 Å simulates the deposition of exfoliated graphene at 300 K.

The structures and properties of these systems were found by density functional theory (DFT) [24,25] using the Vienna *Ab Initio* Simulation Package (VASP) [26]. We used the generalised gradient approximation (GGA), parameterized by Perdew, Burke, and Ernzerhof [27] for the exchange-correlation and the projector augmented-wave method pseudopotentials [28] for carbon. The calculated total energy excludes contributions from the core electrons. In this

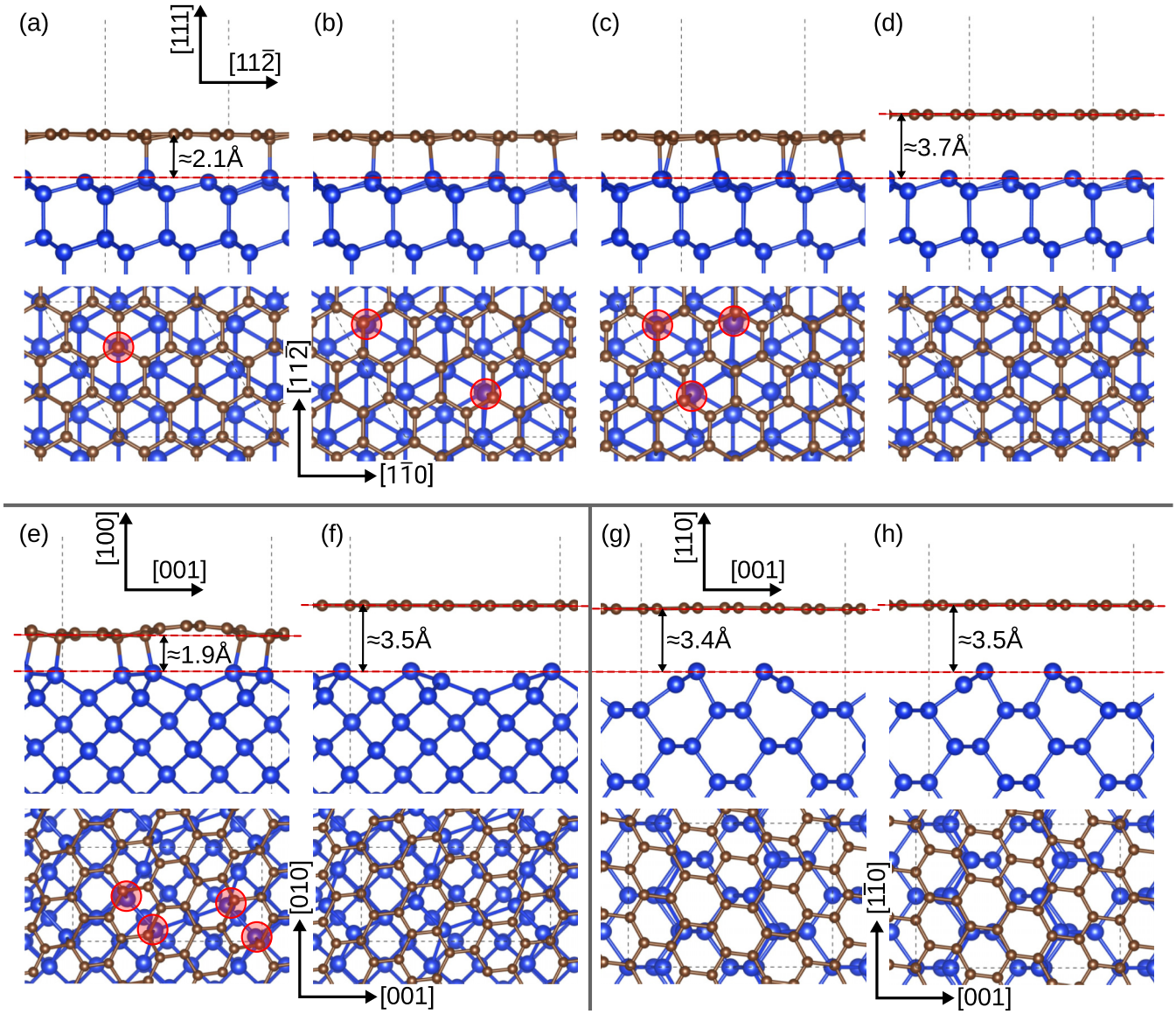

FIG. 1. The relaxed structures of monolayer graphene on various Si surfaces from different initial separations, viewed along the *a* axis (side views), with the corresponding plan views along the *c* axis beneath (which covers a slightly smaller range). (a) Si (111), 1.5 Å; (b) Si (111), 1.5 Å, a different stacking order; (c) Si (111), 1.5 Å, another different stacking order; (d) Si (111), 4.0 Å; (e) Si (100), 1.5 Å; (f) Si (100), 4.0 Å; (g) Si (110), 1.5 Å; (h) Si (110), 4.0 Å. The simulation boxes are labeled by dashed lines. The Si and C atoms forming bonds are labeled by red circles in the plan views.

paper we present the calculated energy relative to the Fermi level ($E - E_F$). The Fermi level calculated by DFT corresponds to the uppermost occupied level at 0 K. We interpret the difference between the Fermi and vacuum levels as the work function, the minimum energy required to remove an electron to the vacuum near the surface. The effects of vdW interactions were included using the Grimme method [29] as implemented in the VASP code. The structural models were visualised using the VESTA software [30]. The uncertainty of the data from the density functional approximation is assessed by comparing the calculated values of pristine graphene in vacuum to the experiments. The calculated work function and carrier density of graphene is lower than the measured value, as expected, due to the effect of substrates and metal contacts [9–12,22].

III. RESULTS AND DISCUSSIONS

A. Interface structure

Figure 1 shows the side views of the relaxed structures of graphene on Si (111) [(a)–(d)], (100) [(e) and (f)], and (110) [(g) and (h)] surfaces, with the corresponding plan views beneath, from two different initial separations, 1.5 Å [(a), (e), and (g)] and 4.0 Å [(d), (f), and (h)]. Note that the relaxed structure possesses high symmetry on Si (111) [the plan view in Fig. 1(a)]. We relaxed the system after several random in-plane displacements of the graphene sheet and obtained two more (meta)stable states [(b) and (c)]. From Figs. 1(d), 1(f), and 1(h), when initially placed far away, a graphene layer can be vdW bonded to all the three orientations of the Si surface, with no visible out-of-plane perturbation (bulging)

on the sp^2 network of graphene. The distance between the graphene plane and the top Si atoms varies between ≈3.5 and ≈3.7 Å. The difference in the distance here can be attributed to the different Si surfaces and the way we define the positions of these surfaces. The Si (111) surface consists of a double-layer [Fig. 1(d)], which is denser and effectively more robust (as the surface is hardly disrupted by the graphene layer above), resulting in a larger interlayer distance with graphene than for the (100) [Fig. 1(f)] and (110) [Fig. 1(h)] surfaces. The larger vdW distance between graphene and Si than between graphene layers in graphite (3.34 Å [18]) indicates a weaker vdW attraction, or that the dangling bonds of Si extend further than the π orbitals of graphene.

The interesting finding here is that when the initial separation between a graphene layer and the Si surface was set to be 1.5 Å, some Si and C atoms approach each other, forming Si-C bonds on the (111) [Figs. 1(a)–1(c)] and (100) surfaces [Fig. 1(e)], but not on the (110) surface [Fig. 1(g)]. On the Si (111) surface, 1 bond per simulation box area is formed [corresponding to a Si-C bond density of 0.018 bond/Å^2, Fig. 1(a)], however, 4 Si-C bonds per simulation box area are formed on the (100) surface [bond density of 0.067 bond/Å^2, Fig. 1(e)]. As a result of more bonds, the interlayer spacing on Si (100) (≈1.9 Å) is smaller than that on Si (111) (≈2.1 Å). In contrast, on the (110) surface, graphene relaxes to a distance of ≈3.4 Å, even from 1.5 Å, and remains visibly flat [Fig. 1(g)]. No Si-C bond is formed on the Si (110) surface. The different vdW distances on the (110) surface from the different initial separations correspond to a difference in energy of 0.07 meV/atom, below the accuracy of the present calculations.

The relaxed structure of graphene on Si (111) possesses high symmetry: one C atom is directly above one Si atom, and the whole model exhibits a 3-fold rotational symmetry along the vertical axis through these vertically overlapping C and Si atoms [Fig. 1(a)]. To understand the effect of stacking orders on the formation of Si-C bonds, we relaxed the structure from additional initial stackings by giving random in-plane translational displacements to the graphene plane within the unit cell dimensions from the high-symmetry structure. With the initial separations at 1.5 Å, two more (meta)stable states were obtained: one with 2 bonds per simulation box area [density of bonds 0.039 bond/Å^2, Fig. 1(b)] and the other with 3 bonds per box area [0.058 bond/Å^2, Fig. 1(c)]. These two additional bonded states on Si (111) are very similar in atomic positions despite different densities of bonds. The relaxations starting at the large separation of 4 Å, but of different initial stackings, always converged to the same state of Fig. 1(d).

We propose a possible interpretation for the formation of these interlayer Si-C bonds: it is related to the surface atom density of the Si substrates. The Si (111) surface consists of a double plane, and is of the highest density. Hence, there is a higher probability of having a Si atom vertically close enough to a C atom, to form a bond. The Si (100) plane is the lowest density, but because of that, atoms at the surface are easily displaced from their original positions and the top two layers merge into one after a graphene layer is placed on top. After the merge, the surface atom density doubles and moreover, compared to the (111) plane, the surface Si atoms

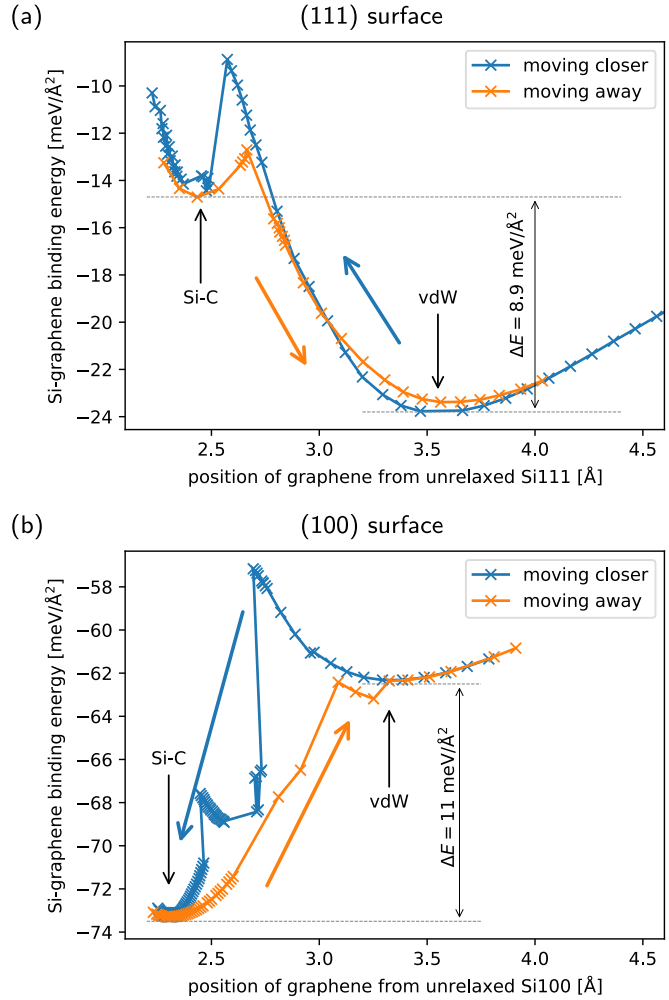

FIG. 2. The binding energy (per in-plane unit area) is plotted against the separation between the graphene and Si surface, on (a) (111) and (b) (100), while displacing the graphene plane towards (blue) and away from (orange) the Si surface. The energies required to form and break the bonds are labeled.

are still quite free to move, further promoting the formation of the bonds. For the (110) plane, its surface is also disrupted by the graphene on top, similarly to the (100) plane, but the low surface atom density further decreases, reducing the chance of forming Si-C bonds. Factors such as surface roughness or surface reconstruction could reduce the effective surface density, further lowering the chance of forming covalent bonds.

B. Interlayer potential

Plotting the interlayer potential energy (binding energy) against interlayer distance (Fig. 2) provides further insights into the significantly different structures of graphene on the different substrates. On the (110) surface, there are no (meta)stable states other than the vdW-bonded state. We investigate the differences in energy and the heights of barriers between (meta)stable states on the (111) and (100) surfaces. We calculated the energy when displacing the graphene layer along the c axis towards, and away from a Si surface. We plotted the interlayer binding energy against the interlayer

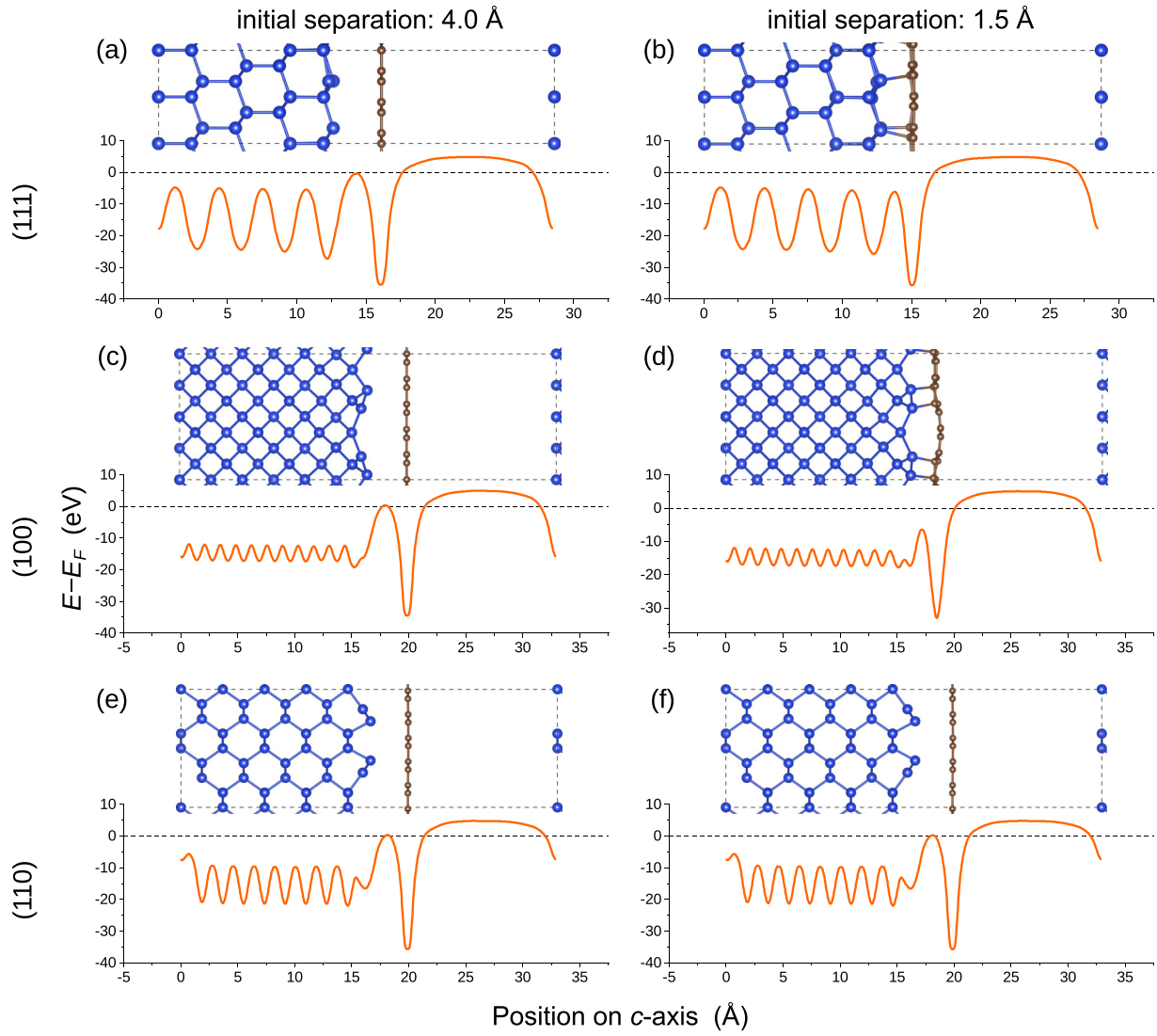

FIG. 3. The difference between the electrostatic potential and the Fermi level is plotted along the c-axis perpendicular to the graphene plane, for graphene on (a) Si (111) with initial separation of 4.0 Å, (b) Si (111) with 1.5 Å, (c) Si (100) with 4.0 Å, (d) Si (100) with 1.5 Å, (e) Si (110) with 4.0 Å, and (f) Si (110) with 1.5 Å. The structures are shown above. The plateau in the energy corresponds to the vacuum between graphene and the first Si layer in the next unit cell. The Fermi level (the zero) is shown by a dashed line.

distance in Fig. 2. At each fixed z coordinates of the corner four C atoms and the fixed positions of the bottom Si layers (note that the plotted distance is to the topmost Si atoms before relaxation, hence different from those labeled in the corresponding structures in Fig. 1), we relaxed the graphene and the top Si layers, and calculated the energy of the relaxed state. From Fig. 2, it is clear that the vdW bonded state is the stable state for graphene on Si (111) and the covalently bonded state is the stable state on Si (100).

In addition to the difference in binding energy between the states, we can also obtain the energy required to form interfacial Si-C bonds relative to the energy at the vdW distance, and that required to break the formed bonds. On the (111) surface, forming Si-C bonds requires 15 meV/Å^2 and breaking these bonds takes only 1.5 meV/Å^2. On the (100) surface, it takes 5 meV/Å^2 to form bonds and 11 meV/Å^2 to break them. On both surfaces, there is a clear hysteresis when moving graphene towards and away from Si. In particular, on the (100) surface, two Si-C bonds (per simulation box) form first before the global minimum energy with four bonds is reached, but there is no intermediate state when breaking these bonds.

C. Work function

We calculated the Fermi level of the system of graphene on Si and plotted the difference between the electrostatic potential energy and the Fermi level along the c axis perpendicular to the graphene plane in Fig. 3. The structures are shown above each plot. The potential wells for the graphene layer are deeper than for the Si layers because there are more C atoms per unit area in a graphene plane than Si atoms in a Si layer. For example, in our simulation unit cell, there are 8 Si atoms in a Si (111) double-layer and 18 C atoms in a graphene plane. The plateau on the right of the graphene corresponds to the vacuum level near the surface, extending to the first Si layer of the next unit cell. The Fermi level (as the zero of

energy) is shown by dashed lines. The work function is here interpreted as the difference between the Fermi level and the electrostatic potential energy in the vacuum. Table I lists the work function values. As mentioned above, the graphene is strained to match the Si lattices, to meet the in-plane periodic boundary condition. The strain modifies the work function of graphene, comparing strained vs. pristine graphene in Table I. We compare the work function of graphene strained to a specific Si surface plane, with and without the actual Si substrate beneath. There are two caveats to mention before we discuss these results. First, the in-plane strain increases the work function significantly [as much as 0.59 eV when strained to Si (100)] compared with unstrained graphene. This is not the center of our interest. Instead, here we focus on the further increase by the presence of Si substrates. Second, because of the anisotropic in-plane strain of graphene to match the Si lattice, there are bandgaps induced in graphene, which are of no interest to this paper. It is how much the Fermi level is shifted into the conduction or valence band that is relevant, and this will be discussed in detail in the next subsection.

The changes of the work function of graphene on Si surfaces at their vdW distances to the graphene planes is 0.27, 0.11, and 0.16 eV on Si (111), (100), and (110) surfaces respectively. The change of the graphene work function can be related to a surface dipole, induced by an asymmetric distribution of electronic orbitals on each side of a graphene layer when placed on a Si surface. The different increases on different Si surface orientations are due to the different electrostatic potentials at the interface of graphene and Si [as shown in Figs. 3(a), 3(c), and 3(e)], to which the work function is sensitive [31], The different local electric fields are a result of different interface structures. The Si (111) surface layer is similar to the layers in the bulk. The top two single-layers at the Si (100) surface merge into one, whilst the surface layer of Si (110) has only about half as many atoms as those in the bulk.

Charge transfer is a common cause for changes of the graphene work function. An important result here is that the Fermi level is very close to the Dirac point of graphene on Si (100) and (110) surfaces, but on the Si (111) surface the Fermi level is shifted by about 0.7 eV into the conduction band. There are 0.037 carbon states/atom between the Dirac point and the shifted Fermi level, whereas an increase of only less than 0.01 state/atom is found in the graphene layer. We propose that the loss of available states below the Fermi level from the significant modification of the DOS of graphene is the main cause of this unconventional doping. It appears that the induced surface dipole from the largely redistributed π orbitals (resulting in significant modification of the density of the π states) increases the work function of graphene on Si (111), overcoming the effect of the shift of the Fermi level. Further discussions follows in the next section after the DOS results are presented.

The work function of graphene is affected most on the most robust (atomically dense) (111) surface and least on the (100) surface, where the atoms are free to move. The robustness can be related to the surface atom density for the three surfaces in this paper. We propose a possible explanation for the effect of the surface orientation. When two very robust surfaces [e.g., graphene and Si (111)] contact, nuclei are held in position by the stable in-plane network of each surface and there will be little disruption on the in-plane structures. With stable nuclear positions, electronic orbitals (especially those out-of-plane, such as the π orbitals of graphene) may significantly redistribute to lower the energy when the graphene approaches a Si surface, inducing surface dipoles or modifying existing ones.

Finally, we consider the effect of graphene forming covalent bonds with Si substrates on the work function of graphene. The work function is increased by 0.02 and 0.11 eV, respectively, on Si (111) and (100) surfaces when covalent bonds are formed, compared to the vdW-bonded states. Forming covalent bonds is a lesser impact than the mere presence of a Si substrate on Si (111), which increases the work function by 0.27 eV. These two have an equal impact on the work function of graphene on Si (100).

D. Carrier density

We obtain the electron (hole) density of graphene by integrating the product of the DOS of all the C atoms and the Fermi-Dirac distribution at 300 K, from the bottom (top) of the conduction (valence) band of graphene to the top (bottom). We choose the DOS of C atoms, because the transport of carriers in C is very different from Si (e.g., in mobility), and we are interested in carriers in the graphene, rather than in the bulk Si. The effect of temperature on the DOS of graphene (and Si) is very small [22]. Here we combine the DOS at 0 K with the Fermi-Dirac distribution at 300 K, to demonstrate the effect of different Si surface orientations on the carrier density of graphene at room temperature. We present the DOS (near the Fermi level) of all the C atoms in each case in Fig. 4. The Fermi levels (dashed lines) are at, or close to, the Dirac point (of zero DOS), except on the (111) surface [Figs. 4(b) and 4(c)]. In Fig. 4(i), there is more than one gap in DOS, and the bandgap due the anisotropic strain is higher in energy than the Fermi level, as its width is consistent with those in Figs. 4(g) and 4(h).

Table I lists the calculated carrier densities. Normally large changes in the carrier density of graphene are achieved by shifting the Fermi level, so the distance of the Fermi level from the edge of the valence or conduction band, whichever is closer, is also listed. In addition to the quantified change in the carrier density of graphene on different surfaces, we also establish that these changes are mainly due to the shift of the Fermi level into the valence or conduction band (as is common), rather than being merely due to the modification of the DOS. The presented distance of the Fermi level to the band edge presented here is the relevant quantity, and this is not affected by the widths of the bandgaps.

The uncertainty of the data is as follows. The edge of the valence and conduction bands was read from the DOS in Fig. 4. The interval between the calculated data points of the DOS is about 0.04 eV. The Fermi-Dirac distribution at 300 K (the temperature has a very small effect on the DOS) decays so fast that its value may already decrease from 0.5 at the Fermi level to 0.2 at the closest data point, and most of the carrier density is contributed from the closest three data points near the Fermi level on one side. We use two approaches to calculate the carrier density. One is to linear fit the closest five data points to the Fermi level on one side

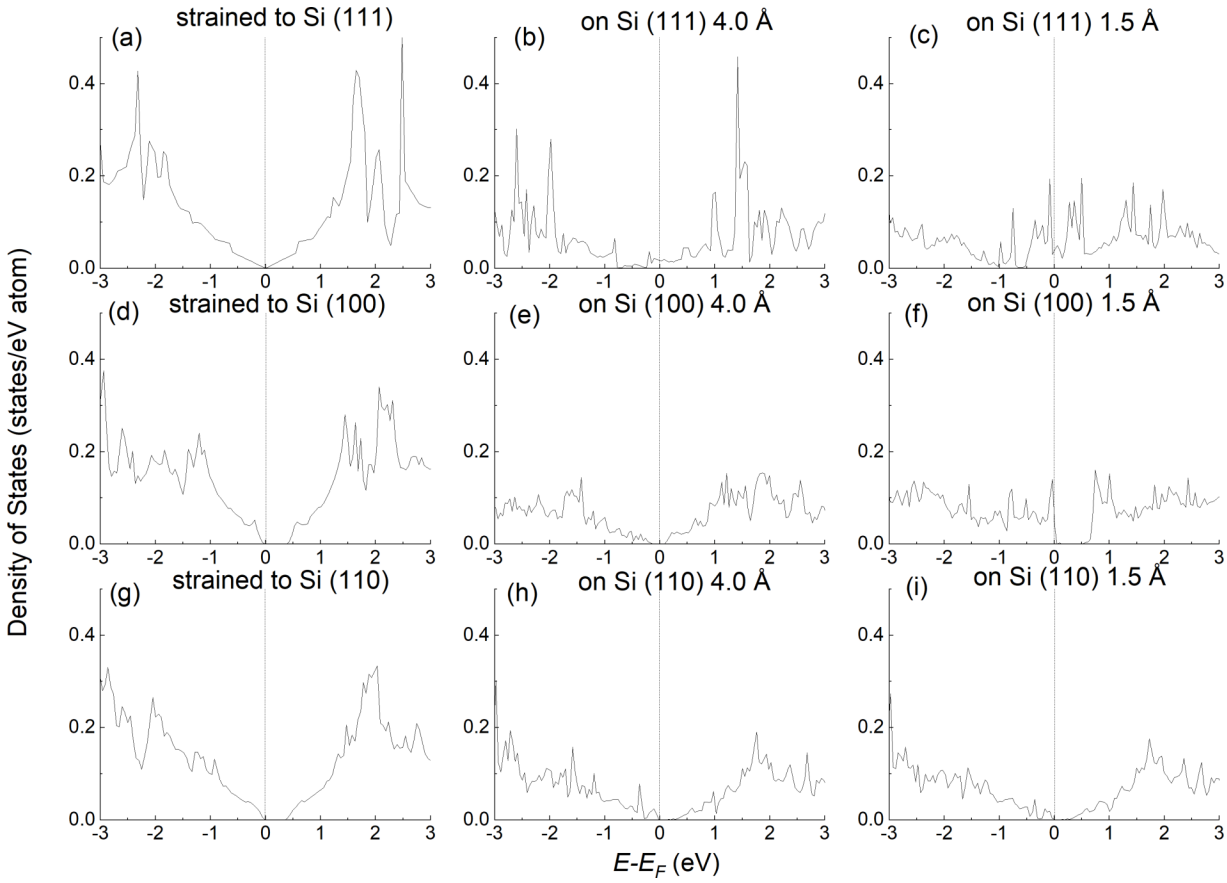

FIG. 4. The densities of states (per atom, around the Fermi levels of the systems) of the carbon atoms are plotted, for graphene (a) strained to Si (111) but unsupported, (b) on Si (111) with an initial separation of 4.0 Å, (c) on Si (111) with 1.5 Å, (d) strained to Si (100) but unsupported, (e) on Si (100) with 4.0 Å, (f) Si (100) with 1.5 Å, (g) strained to Si (110) but unsupported, (h) Si (110) with 4.0 Å, and (i) Si (110) with 1.5 Å. Energy is referenced to the Fermi levels, which is shown by the chain-dotted lines at $E - E_F = 0$.

to obtain an analytical form of the DOS and to integrate over this small range. The other is to sum up areas of rectangles from the edge of band to the other end. The difference of these two approaches is about 10%, which is one source of the uncertainty. There is a further uncertainty due to some of the interstitial states between graphene and Si being wrongly projected to Si, which could modify the presented values of carrier density by a factor of 2 at most. And we make the assumption that the distance of the Fermi level to the band edge is not affected by the width of the bandgap from the imposed anisotropic in-plane strain. When the Fermi level is calculated to lie within the bandgap, we consider the graphene to be undoped. This assumption potentially further increases the uncertainty of the data, and we therefore only focus on the changes by orders of magnitude.

The Fermi level of the unsupported graphene is at the Dirac point (despite the in-plane strain), as expected. The carrier densities of electrons and holes are the same and the values are consistent with those reported in the literature [19,22,32]. The in-plane strain does not affect the carrier density, which is reasonable as the states near the Dirac point are all from the out-of-plane π-electronic orbitals. When the graphene is placed on the Si (111) surface at the vdW distance, the Fermi level is shifted by 0.7 eV into the conduction band from the Dirac point, resulting in an increase of the electron density by more than two orders of magnitude. When a covalent bond is formed to the Si (111) surface, the Fermi level is shifted slightly less into the conduction band (by 0.6 eV), but to an energy range where the graphene DOS is large, resulting in an increase of carrier density by three orders of magnitude.

The significant increase in the charge density (and the work function from the previous section) is due to an unconventional n-type doping, which is not due to charge transfer, but to a modification of the DOS. The shift of the Fermi level into the conduction band is unexpected, as the Fermi level of the system (graphene placed on Si) is higher than both the Dirac point of graphene and the top of the valence band of Si. A possible explanation is that the number of available states of graphene and/or Si below the Dirac point of graphene has decreased, due to the interaction between the graphene and Si surface. This is a new mechanism of doping, that is determined by the surface orientation and density of a crystal substrate.

On Si (100) and (110) surfaces, bandgaps of graphene from the anisotropic strain are of no interest in this paper. With the Fermi levels remaining at the edge of the bands, the carrier densities are of the same magnitude as that of pristine graphene, except when the graphene is covalently bonded to the Si (100) surface. Here the DOS increases sharply near

the Dirac point [Fig. 4(f)], which results in an increase of the carrier density by a factor of 80.

The larger the Si surface atom density, the more it can modify the π-orbitals and the DOS of graphene. The carrier density of graphene on Si (100) is therefore greatly increased, and it can be further increased on Si (111) (with the highest surface atom density), where the Fermi level is shifted through the modification of the DOS.

IV. CONCLUSIONS

In this paper, we modelled monolayer graphene on Si substrates having three different surface orientations, (111), (100), and (110). We found that the role of the substrate is remarkably varied according to its orientation. We simulated close approaches of carbon atoms to Si, that could be reached under the high growth temperature, as well as the vdW distance from the deposition of exfoliated graphene at room temperature. Even when the interaction with the graphene is only vdW, there can be large modifications to the graphene DOS, leading to large effects (work function and carrier density). The formation of Si-C covalent bonds is also highly orientation-dependent. We relate these effects to the surface atom density of Si substrates and demonstrate the underlying physics. In particular, we propose a mechanism of an unconventional doping, that is due to the modification of the DOS, which requires high surface atomic density of a substrate. Our findings further help to understand the effects of surface roughness and reconstruction.

ACKNOWLEDGMENTS

Y.W.S. is grateful for the valuable discussion with Dr. Dimitrios Papageorgiou, Dr. Jan Mol from Queen Mary University of London, and Dr. Wei Liu from Zhejiang University. Y.W.S., O.F., and C.J.H. are grateful for the financial support from the Innovate UK [Project No. 104714]. O.F. is a Royal Society University Research Fellow (UF140372; URFR201013). The computational results presented have been achieved [in part] using the Viennaao Scientific Cluster (VSC).

[1] K. S. Novoselov, A. K. Geim, S. V. Morozov, D. Jiang, Y. Zhang, S. V. Dubonos, I. V. Grigorieva, and A. A. Firsov, Science **306**, 666 (2004).
[2] M. Saeed, Y. Alshammari, S. A. Majeed, and E. Al-Nasrallah, Molecules **25**, 3856 (2020).
[3] Z. Chen, C. Xie, W. Wang, J. Zhao, B. Liu, J. Shan, X. Wang, M. Hong, L. Lin, L. Huang *et al.*, Sci. Adv. **7**, eabk0115 (2021).
[4] Z. Weng, S. C. Dixon, L. Y. Lee, C. J. Humphreys, I. Guiney, O. Fenwick, and W. P. Gillin, Adv. Opt. Mater. **10**, 2101675 (2022).
[5] D. Zhu, D. J. Wallis, and C. J. Humphreys, Rep. Prog. Phys. **76**, 106501 (2013).
[6] W. Zhu, V. Perebeinos, M. Freitag, and P. Avouris, Phys. Rev. B **80**, 235402 (2009).
[7] E. H. Hwang, S. Adam, and S. Das Sarma, Phys. Rev. Lett. **98**, 186806 (2007).
[8] P. A. Khomyakov, G. Giovannetti, P. C. Rusu, G. Brocks, J. van den Brink, and P. J. Kelly, Phys. Rev. B **79**, 195425 (2009).
[9] R. Yan, Q. Zhang, W. Li, I. Calizo, T. Shen, C. A. Richter, A. R. Hight-Walker, X. Liang, A. Seabaugh, D. Jena *et al.*, Appl. Phys. Lett. **101**, 022105 (2012).
[10] S. M. Song, J. K. Park, O. J. Sul, and B. J. Cho, Nano Lett. **12**, 3887 (2012).
[11] S. Song and B. Cho, Carbon Lett. **14**, 162 (2013).
[12] J. K. Park, S. Song, J. Mun, and B. Cho, Nano Lett. **11**, 5383 (2011).
[13] A. Comas-Vives, Phys. Chem. Chem. Phys. **18**, 7475 (2016).
[14] Y. Song, X. Li, C. Mackin, X. Zhang, W. Fang, T. Palacios, H. Zhu, and J. Kong, Nano Lett. **15**, 2104 (2015).
[15] K. K. Kim, A. Reina, Y. Shi, H. Park, L. J. Li, Y. H. Lee, and J. Kong, Nanotechnology **21**, 285205 (2010).
[16] S. Ryu, L. Liu, S. Berciaud, Y. J. Yu, H. Liu, P. Kim, G. W. Flynn, and L. E. Brus, Nano Lett. **10**, 4944 (2010).
[17] D. Xu, X. Yu, L. Yang, and D. Yang, Superlattices Microstruct. **99**, 3 (2016).
[18] F. Tuinstra and J. L. Koenig, J. Chem. Phys. **53**, 1126 (1970).
[19] T. Fang, A. Konar, H. Xing, and D. Jena, Appl. Phys. Lett. **91**, 092109 (2007).
[20] P. P. Altermatt, J. Appl. Phys. **93**, 1598 (2003).
[21] O. Madelung, U. Rossler, and M. Schulz, *Germanium, Intrinsic Carrier Concentration* (Springer Materials, New York, 2002)
[22] Y. Yin, Z. Cheng, L. Wang, K. Jin, and W. Wang, Sci. Rep. **4**, 5758 (2014).
[23] C. M. Zetterling, *Process Technology for Silicon Carbide Devices* (INSPEC, London, 2002).
[24] P. Hohenberg and W. Kohn, Phys. Rev. **136**, B864 (1964).
[25] W. Kohn and L. Sham, Phys. Rev. **140**, A1133 (1965).
[26] G. Kresse and J. Furthmüller, Phys. Rev. B **54**, 11169 (1996).
[27] J. P. Perdew, K. Burke, and M. Ernzerhof, Phys. Rev. Lett. **77**, 3865 (1996).
[28] G. Kresse and D. Joubert, Phys. Rev. B **59**, 1758 (1999).
[29] S. Grimme, J. Comput. Chem. **27**, 1787 (2006).
[30] K. Momma and F. Izumi, J. Appl. Crystallogr. **44**, 1272 (2011).
[31] J. Bardeen, Phys. Rev. **71**, 717 (1947).
[32] L. Wang, W. Wang, G. Xu, Z. Ji, N. Lu, L. Li, and M. Liu, Appl. Phys. Lett. **108**, 013503 (2016).